JOURNAL OF SPACECRAFT AND ROCKETS
Vol. 39, No. 5, September–October 2002

Modeling a Piezothermoelastic Beam String

James W. Rogers Jr.*
U.S. Air Force Research Laboratory, Wright–Patterson Air Force Base, Ohio 45433
and
Gregory S. Agnes†
U.S. Air Force Institute of Technology, Wright–Patterson Air Force Base, Ohio 45433

An analysis of laminated piezopolymer-actuated flexible beams is presented. Complete development of the nonlinear equations of motion governing a continuous, slender, laminate of arbitrary thermal, mechanical, and electrical properties is presented. A closed-form asymptotic solution is developed using a combination or perturbation techniques. These governing equations are applied to a pressurized simple piezoelectrically actuated Kapton® material model. Both static and dynamic results indicate shape control at optical wavelengths is possible.

Nomenclature

A	=	cross-sectional area
c_1, c_2	=	axial, transverse speed of sound
D	=	differential
$\mathrm{d}s$	=	deformed segment length
$\mathrm{d}x$	=	undeformed segment length
d_{31}	=	piezoelectric constant
E	=	Young's modulus
EA	=	axial stiffness
EA_z	=	unsymmetrical axial stiffness
EA_ϵ	=	prestress axial stiffness contribution
$EA_{\epsilon z}$	=	prestress unsymmetrical axial stiffness contribution
EI	=	bending stiffness
f, f_0	=	half amplitude, bias of applied force
g	=	independent variable (x, R, t)
K_{eff}	=	exterior membrane effective stiffness
K_0, K_L	=	end torsional spring constants
L	=	beam length
M_P	=	piezoelectric moment contribution
m, m_0	=	half amplitude, bias of applied moment
N_i	=	initial axial load
N_P	=	piezoelectric tension contribution
N_0	=	initial tension
P	=	pressure differential
q	=	order
R	=	membrane radial dimension
R^*	=	radius of electroded region
r	=	radius of gyration
T	=	timescales
$\mathbb{T}$	=	kinetic energy
$\mathcal{T}$	=	temperature
t	=	time
t^*	=	beam thickness
u, w	=	displacements
V	=	applied voltage
$\mathbb{V}$	=	potential energy
$\mathcal{V}$	=	integration volume
$\mathbb{W}_{\text{nc}}$	=	nonconservative work
x, z	=	reference axes
α	=	thermal constant
β	=	modal frequencies
δ	=	detuning parameter
ϵ	=	strain
ε	=	expansion parameter
ϵ_0	=	prestrain
ζ	=	stretching variable $(x = L)$
μ	=	transverse damping factor
ν_u	=	axial damping factor
ξ	=	stretching variable $(x = 0)$
ρ	=	beam material density
σ	=	stress
σ_0	=	prestress
τ	=	scaled time
Ω	=	center frequency
ω	=	frequency expansion

Subscripts

$,g$	=	derivative with respect to variable g
q	=	order notation

Superscript

T	=	transpose

Introduction

THE largest space-based optical reflector launched to date is the Hubble space telescope with a primary reflector of nearly 2.4 m. A larger aperture (8 m) is required for the Next Generation Space Telescope, requiring a deployable solution. Advanced radio interferometry between space and earth (ARISE), another space telescope effort, is currently underway to investigate inflatable reflector designs that can easily fit within the current launch vehicle weight and volume constraints.

During the past 15 years, a resurgence of inflatables technology has occurred resulting in the deployment of the IN-STEP inflatable antenna experiment in 1996 (Ref. 1). Although problems occurred during deployment, this experiment validated many technologies.[2] The 14-m inflatable reflector, including inflatable struts, was packaged inside a $2.0 \times 1.1 \times 0.5$ m^3 ($80 \times 43 \times 21$ in.^{3}) canister and deployed during the NASA space shuttle mission STS-77 (Fig. 1).

Additional flexibility is accompanied with additional problems. As the wavelength of the collected signal decreases, the reflector's allowable shape error decreases. Thus, a large reflector used to collect radio frequency signals does not need nearly the precision as does an optical reflector. An optical reflector must produce a wavefront without significant distortion, or phase error, when received at the sensor.

Current reflector designs use extremely thin ($\sim$50-μm) polyimide-type materials stretched over extremely large distances ($\sim$20 m). Shape and vibration control of these large membranes

Received 26 June 2001; revision received 8 April 2002; accepted for publication 20 May 2002.

*Aeronautical Engineer, AFRL/VASS; james.rogers2@wpafb.af.mil. Member AIAA.

†Assistant Professor, Department of Aeronautics and Astronautics; gregory.agnes@afit.edu. Member AIAA.

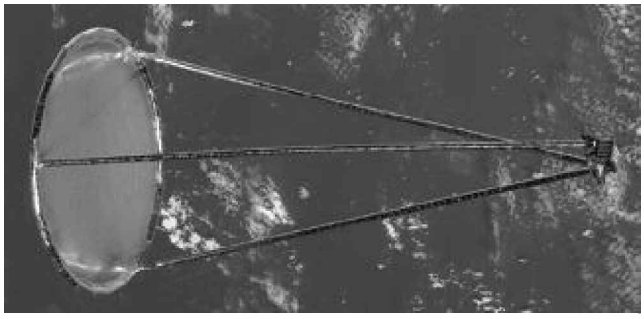

Fig. 1 IN-STEP spacecraft.

must be accomplished if a viable solution can be expected. Research currently underway at the Air Force Institute of Technology (AFIT) addresses the shape and vibration control of membranes for applications at optical wavelengths. Experimental results included the development of an optical measurement capability using interferometry and wave front analysis of a 0.15-m membrane mirror test subject.[3]

After a short discussion of a linear axisymmetric membrane, this paper presents the development of one-dimensional, nonlinear piezothermoelastic beam equations of motion. With the use of asymptotic methods, the static and dynamic solutions to this system is achieved and discussed.

Active Membranes

With the use of a membrane material, such as Upilex (a polyiminde), metalized on one side to provide the necessary reflective surface, a membrane mirror can be created. When a laminate of polyvinylidine fluoride (PVDF) layers is applied on the nonreflective side, an active membrane reflector can be constructed. PVDF is a piezoelectric polymer that strains when an electrical potential is applied across the thickness. In general, this effect is orthotropic, resulting in much smaller effects in the transverse direction, but bidirectional PVDF is also available. Conceivably, two layers of PVDF can be used to produce a bimorph effect. If the two layers strain differently, curvature results. Applying a single layer of PVDF to Upilex and applying a time periodic electrical potential near the composite membrane's natural frequency produces significant deformation. Because of the directional properties of PVDF, a laminate of angled layers is being considered by the AFIT to provide desired controllability for a two-dimensional membrane surface.

Previous experimental results clearly indicate surface "print-through" wherever there is a material or electrical discontinuity.[3] This print-through is a physical distortion of the reflective surface resulting from the forces experienced on the reverse side. Although the distortion area is very small for a given disturbance, these disturbances may occur throughout the surface due to the control necessary across the entire surface. When perfect bonding is assumed between layers, these discontinuities exist wherever the laminate physically changes or the electrical potential changes, for example, electrode edge regions. Print-through is also significant at this time due to laminating procedure techniques. Adhesive application is uneven and causes significant surface distortion, but acceptable distortion magnitude is still under evaluation at AFIT. Errors visible to the naked eye are obviously unacceptable because the precision required is on the order of optical wavelengths (~600 nm).

Current efforts are also underway at the University of Kentucky.[4] When a PVDF backing on an optical membrane is used, an electron gun is used to apply the electrical potential that causes the surface deformation. The authors are unaware of any optical wave front measurements of this surface.

Additionally, when considering space environment applications, substantial thermal variations are expected. The design and implementation of an active membrane requires a new set of analytical tools. A finite element modeling capability providing thermal, electrical, and mechanical evaluation is currently in development at AFIT for just this purpose. When asymptotic methods are used, this development will provide insight into the behavior of these materials and support the design of the shape and vibration controllers necessary for optical performance.

Experimental validation will also be required. Analytical results using asymptotic methods will also provide a necessary initial validation. This paper represents the first step toward this end: the asymptotic solution for a piezoelectric beam undergoing moderate deformation. A beam was selected due to the similarity between axisymmetric membrane solutions and one-dimensional beam strings. To further clarify the relationship, a short linear membrane discussion is presented next.

Linear Axisymmetric Piezoelastic Membrane

Agnes and Wagner presented a simplified linear membrane analysis modeling the effects of a piezoelectric allaminate when applied to a nonpressurized axisymmetric circular membrane.[5] Figure 2 shows the laminated membrane configuration with cross section modeled as shown in Fig. 3. When a uniform radial tension is assumed with axisymmetric boundary conditions, the equations of motion for the symmetric response are

$$D^*\nabla^4 W(R) - N\nabla^2 W(R) = 0 \tag{1}$$

where

$$D^* = \sum_i \int_{t_i^*} \frac{E_i z^2}{4(1-\nu^2)}\,\mathrm{d}z \tag{2}$$

$$N = N_0 + N_P \tag{3}$$

$$\nabla^2 = \frac{\partial^2}{\partial R^2} - \frac{1}{R}\frac{\partial}{\partial R} \tag{4}$$

Note that $\nabla^4 = \nabla^2(\nabla^2)$ and that the boundary conditions are

$$W(0) < \infty \tag{5}$$

$$W_{,R}(0) = 0 \tag{6}$$

$$W(R^*) = 0 \tag{7}$$

$$EIW_{,RR} = M_P + K_{\text{eff}} W_{,R} \tag{8}$$

When a matched asymptotic expansion perturbation analysis is applied to account for the boundary area effects, the deflection of the circular membrane to second order is

$$w(R) = -\varepsilon^2\left(M_P R^*/EI\right)(1 - e^{\eta}) + \mathcal{O}(\varepsilon^3) \tag{9}$$

where $\varepsilon^2 = D^*/R^*N_0$ and $\eta = (R - R^*)/\varepsilon R^*$.

The response consists of a sharp bend at the boundary followed by a flat displacement (almost pistoning) of the center region. The smallness term ε is directly related to the membrane's radius of

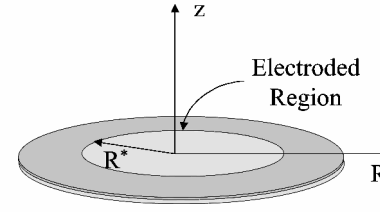

Fig. 2 Piezoelastic membrane.

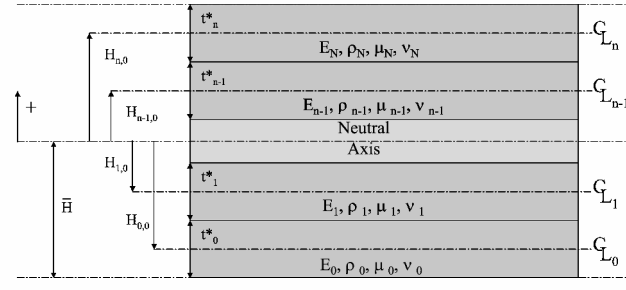

Fig. 3 Piezoelectric laminate cross section.

gyration, which becomes very small in the applications considered here, and indicates the size of the actual boundary region. Piezoelectric actuation of a thin membrane, thus, is seen to induce only localized curvature in the membrane near the edge of the electroded region. Within that region, away from these edge regions, the tension of the membrane is adjusted, and the membrane deflects uniformly. This was a simplified linear analysis that ignored many nonlinear effects including in-plane stretching and possible transverse pressure conditions. With the recognition that axisymmetric systems often reduce to one-dimensional problems, a nonlinear analysis of a flexible beam can provide significant insight into the nonlinear effects brought about due to the nonlinear terms ignored in linear analysis.

Laminated Piezothermoelastic Beam String

To develop the necessary fundamental equations used in this analysis, an energy-based derivation can be used. Refer to Figs. 3 and 4 throughout the following derivation. The potential energy of an elastic beam can be defined using the strain energy representation[6]

$$\mathbb{V} = \int_{\mathcal{V}} \frac{1}{2}\{\epsilon\}^T\{\sigma\} - \{\epsilon\}^T\{\sigma_0\} + \{\epsilon_0\}^T\{\sigma\}\,\mathrm{d}\mathcal{V}$$

$$+ \frac{1}{2}K_0 w_{,x}(0,t)^2 + \frac{1}{2}K_L w_{,x}(L,t)^2 \tag{10}$$

with

$$\sigma = [E]\{\epsilon\}, \qquad \sigma_0 = \frac{N_i}{A} \tag{11}$$

$$\epsilon = \frac{\mathrm{d}s - \mathrm{d}x}{\mathrm{d}x} - z w_{,xx}, \qquad \epsilon_0 = \alpha\mathcal{T} + \frac{d_{31}V}{t^*} \tag{12}$$

The addition of the spring constants K_0 and K_L at each end of the beam allows for variable boundary conditions used later in the analysis. The beam's kinetic energy can be represented as

$$\mathbb{T} = \frac{1}{2}\int_{\mathcal{V}} \rho\left(u_{,t}^2 + w_{,t}^2\right)\mathrm{d}\mathcal{V} \tag{13}$$

The system's nonconservative work from the follower pressure force can be approximated assuming the deflections are small with respect to the overall dimensions. A corresponding expansion can be created and then truncated to produce

$$\mathbb{W}_{\mathrm{nc}} = -\int_x P(w + u_{,x}w - w_{,x}u)\,\mathrm{d}x \tag{14}$$

To analyze a laminate, further analysis is required. Refer to Fig. 3; each layer can have independent elastic, thermal, and piezoelectric properties. When it is assumed that through-the-thickness strain is constant at any cross section, the system can be collapsed to a one-dimensional integrodifferential equation. With the application of Hamilton's principle,

$$\int_{t_1}^{t_2} \delta\mathbb{T} - \delta\mathbb{V} + \delta\mathbb{W}_{\mathrm{nc}}\,\mathrm{d}t = 0 \tag{15}$$

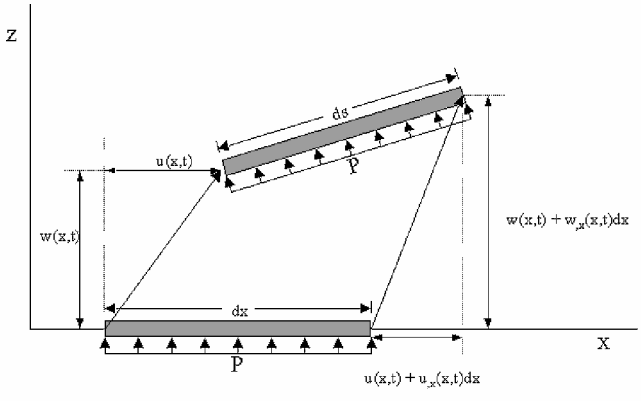

Fig. 4 Pressurized beam deflection.

where δ in this equation indicates variation, the following dimensional system is derived:

$$\rho A u_{,tt} - EA u_{,xx} = \frac{1}{2}(EA - N)\frac{\partial}{\partial x}\left(w_{,x}^2 - 2u_{,x}w_{,x}^2\right) - 2Pw_{,x}$$

$$- EA_z\frac{\partial}{\partial x}\left[w_{,xx}\left(1 - \frac{1}{2}w_{,x}^2 + u_{,x}w_{,x}^2\right)\right] \tag{16}$$

$$\rho A w_{,tt} - N w_{,xx} + EI w_{,xxxx} = (EA - N)\frac{\partial}{\partial x}(e w_{,x})$$

$$+ P(1 - 2u_{,x}) - EA_z\frac{\partial}{\partial x}\left[u_{,xx}\left(1 - \frac{1}{2}w_{,x}^2 + u_{,x}w_{,x}^2\right)\right] \tag{17}$$

$$e = u_{,x} - u_{,x}^2 + \frac{1}{2}w_{,x}^2 \tag{18}$$

$$N = N_i - EA_\epsilon \tag{19}$$

with the following boundary conditions of interest:

$$EI w_{,xx} - N_z + EA_{\epsilon z} = K_L w_{,x}$$

$$+ EA_z\left(u_{,x} + \tfrac{1}{2}w_{,x}^2 - \tfrac{1}{8}w_{,x}^4 - \tfrac{1}{2}u_{,x}w_{,x}^2 + \tfrac{1}{2}u_{,x}^2 w_{,x}^2\right)\Big|_{x=L} \tag{20}$$

$$EI w_{,xx} - N_z + EA_{\epsilon z} = -K_0 w_{,x}$$

$$+ EA_z\left(u_{,x} + \tfrac{1}{2}w_{,x}^2 - \tfrac{1}{8}w_{,x}^4 - \tfrac{1}{2}u_{,x}w_{,x}^2 + \tfrac{1}{2}u_{,x}^2 w_{,x}^2\right)\Big|_{x=0} \tag{21}$$

The parameters are defined as

$$\rho A = \int_A \rho\,\mathrm{d}A, \qquad N_z = \int_A \frac{N_i}{A} z\,\mathrm{d}A, \qquad EA = \int_A E\,\mathrm{d}A$$

$$N_0 = \int_A \frac{N_i}{A}\,\mathrm{d}A, \qquad EA_\epsilon = \int_A E\epsilon_0\,\mathrm{d}A, \qquad EA_{\epsilon z} = \int_A E\epsilon_0 z\,\mathrm{d}A$$

$$EI = \int_A E z^2\,\mathrm{d}A, \qquad EA_z = \int_A E z\,\mathrm{d}A \tag{22}$$

If all measurements are with respect to the original neutral axis of a symmetric laminate (N_z, $EA_z \to 0$), Eqs. (16) and (17) are the same as presented by Nayfeh and Mook[7] with additional pressure terms. Notice that the thermal and piezoelectric terms not only modify the axial tension within the beam, but also produce moments at the boundary, that is, $EA_{\epsilon z}$.

To perform a perturbation analysis of this system properly, the system must be put in nondimensional form. The following nondimensional parameter scaling rules are used:

$$\hat{x} = x/L, \qquad \hat{z} = z/L, \qquad \hat{u} = u/L, \qquad \hat{w} = w/L$$

$$\hat{r}^2 = (EI/L^2EA)\left(c_1^2/c_2^2\right), \qquad \hat{P} = (PL/EA)\left(c_1^2/c_2^2\right)$$

$$\hat{N}_0 = c_2^2/c_1^2, \qquad \hat{N}_z = (N_z/LEA)\left(c_1^2/c_2^2\right)$$

$$\hat{EA}_z = (EA_z/LEA)\left(c_1^2/c_2^2\right), \qquad \hat{EA}_{\epsilon z} = (EA_{\epsilon z}/LEA)\left(c_1^2/c_2^2\right)$$

$$\hat{K}_1 = (K_L/LEA)\left(c_1^2/c_2^2\right), \qquad \hat{K}_0 = (K_0/LEA)\left(c_1^2/c_2^2\right)$$

$$\hat{EA}_\epsilon = (EA_\epsilon/EA)\left(c_1^2/c_2^2\right), \qquad \hat{t}^2 = \left(c_2^2/L^2\right)t^2$$

where $c_1^2 = EA/\rho A$ and $c_2^2 = N_0/\rho A$, to produce (eliminating the carets)

$$u_{,tt} - \frac{c_1^2}{c_2^2}u_{,xx} = -2Pw_{,x} - 2v_u u_{,t}$$

$$+ \frac{1}{2}\left(\frac{c_1^2}{c_2^2} - 1 + EA_\epsilon\right)\frac{\partial}{\partial x}\left(w_{,x}^2 - 2u_{,x}w_{,x}^2\right)$$

$$- EA_z\frac{\partial}{\partial x}\left[w_{,xx}\left(1 - \frac{1}{2}w_{,x}^2 + u_{,x}w_{,x}^2\right)\right] \tag{23}$$

$$w_{,tt} - (1 - EA_\epsilon)w_{,xx} + r^2 w_{,xxxx} = -2\mu w_{,t} + \left(\frac{c_1^2}{c_2^2} - 1 + EA_\epsilon\right)\frac{\partial}{\partial x}(e w_{,x}) + P(1 - 2u_{,x}) - EA_z \frac{\partial}{\partial x}\left[u_{,xx}\left(1 - \frac{1}{2}w_{,x}^2 + u_{,x}w_{,x}^2\right)\right] \tag{24}$$

$$e = u_{,x} - u_{,x}^2 + \frac{1}{2}w_{,x}^2 \tag{25}$$

with boundary conditions

$$r^2\left(c_2^4/c_1^4\right)w_{,xx} - N_z + EA_{\epsilon z} + \hat{K}_0 w_{,x} = EA_z\left(u_{,x} + \tfrac{1}{2}w_{,x}^2 - \tfrac{1}{8}w_{,x}^4 - \tfrac{1}{2}u_{,x}w_{,x}^2 + \tfrac{1}{2}u_{,x}^2 w_{,x}^2\right)\Big|_{x=0} \tag{26}$$

$$r^2\left(c_2^4/c_1^4\right)w_{,xx} - N_z + EA_{\epsilon z} - \hat{K}_L w_{,x} = EA_z\left(u_{,x} + \tfrac{1}{2}w_{,x}^2 - \tfrac{1}{8}w_{,x}^4 + \tfrac{1}{2}u_{,x}w_{,x}^2 + \tfrac{1}{2}u_{,x}^2 w_{,x}^2\right)\Big|_{x=1} \tag{27}$$

where ν_u and μ are added as axial and transverse damping values. The system is now normalized in time to the fundamental transverse frequency of the beam. Notice that the normalized axial frequency is the ratio of the transverse and axial speeds of sound. Because $c_2/c_1 = \sqrt{(N_0/EA)}$, we can see the direct result the pretension causes when applied in a perturbation expansion.

Now, define all measurements from the neutral axis, which eliminates the N_z terms, and apply perturbation techniques: A system of linear equations can be developed. The solution presented was developed using a combination of three standard perturbation techniques: Lindstedt–Poincaré, multiple timescales, and matched asymptotic expansions (see Ref. 8). Using the expansions

$$\tau = \omega t, \qquad T_n = \varepsilon^n \tau, \qquad \omega = \omega_0 + \varepsilon\omega_1 + \varepsilon^2\omega_2 + \cdots$$
$$w(x, \tau; \varepsilon) = \varepsilon^2 w_2(x, \tau) + \varepsilon^3 w_3(x, \tau) + \varepsilon^4 w_4(x, \tau) + \cdots$$
$$u(x, \tau; \varepsilon) = \varepsilon^3 u_3(x, \tau) + \varepsilon^4 u_4(x, \tau) + \varepsilon^5 u_5(x, \tau) + \cdots$$
$$D = D_0 + \varepsilon D_1 + \varepsilon^2 D_2 + \cdots, \qquad \varepsilon = r \tag{28}$$

we simultaneously apply Lindstedt–Poincaré and multiple timescale methods. Applying the scaling results to the system of linear partial differential equations, we can model the original nonlinear system. The axial deflection is expected to be much smaller than the transverse and is scaled as such.

Using the matched asymptotic expansion method with the multiple scales method,[8] we can develop a solution that illustrates the stringlike behavior in the center of the beam, with small boundary regions that act as a beam. By the application of the expansions [Eqs. (28)] to Eqs. (23–25) then the extraction of equations based on the relative order, the following system of equations is derived for the outer solution (related to the center portion of the beam string):

$$u_{3,00} - \left(c_1^2/c_2^2\right)u_{3,xx} = 0 \tag{29}$$

$$u_{4,00} - \left(c_1^2/c_2^2\right)u_{4,xx} = -2u_{3,01} - 2\omega_1 u_{3,00} - 2\nu_{u1}u_{3,0} - 2P_2 w_{2,x} + \tfrac{1}{2}\left[\left(c_1^2/c_2^2\right) - 1\right]\left(w_{2,x}^2\right)_{,x} - EA_{z2}w_{2,xxx} \tag{30}$$

$$u_{5,00} - \left(c_1^2/c_2^2\right)u_{5,xx} = -2u_{4,01} - 2\omega_1 u_{4,00} - 2\nu_{u1}u_{4,0} - 2P_2 w_{3,x} - 2u_{3,02} - u_{3,11} - 4\omega_1 u_{3,01} - \left(\omega_1^2 + 2\omega_2\right)u_{3,00} - 2\nu_{u1}u_{3,1} - 2\omega_1\nu_{u1}u_{3,0} + \left(c_1^2/c_2^2\right)(w_{2,x}w_{3,x})_{,x} - EA_{z2}w_{3,xxx} \tag{31}$$

$$w_{2,00} - w_{2,xx} = P_2 \tag{32}$$

$$w_{3,00} - w_{3,xx} = -2w_{2,01} - 2\omega_1 w_{2,00} - 2\mu_1 w_{2,0} \tag{33}$$

$$w_{4,00} - w_{4,xx} = -w_{2,11} - 2w_{0,02} - 4\omega_1 w_{2,01} - \left(\omega_1^2 + 2\omega_2\right)w_{2,00} - 2\mu_1 w_{2,1} - 2\omega_1\mu_1 w_{2,0} - 2w_{3,01} - 2\omega_1 w_{3,00} - 2\mu_1 w_{3,0} - EA_{\epsilon 2}w_{2,xx} - w_{2,xxxx} \tag{34}$$

These equations indicate that, in the outer region of the beam, the dynamic shape of the beam appears much as a string. Next, stretch the x dimension near one end (we will first look at $x = 0$) to create the inner solution near that end of the beam. When the stretched variable $\xi = x/\varepsilon$ is applied, the following system is derived for the region near the $x = 0$ end of the beam:

$$-\left(c_1^2/c_2^2\right)u_{3,\xi\xi} = \tfrac{1}{2}\left[\left(c_1^2/c_2^2\right) - 1\right]\left(w_{2,\xi}^2\right)_{,\xi} - EA_{z2}w_{2,\xi\xi\xi} \tag{35}$$

$$-\left(c_1^2/c_2^2\right)u_{4,\xi\xi} = \left[\left(c_1^2/c_2^2\right) - 1\right](w_{2,\xi}w_{3,\xi})_{,\xi} - EA_{z2}w_{3,\xi\xi\xi} \tag{36}$$

$$-\left(c_1^2/c_2^2\right)u_{5,\xi\xi} = -u_{3,00} - 2P_2 w_{2,\xi} + \tfrac{1}{2}\left[\left(c_1^2/c_2^2\right) - 1\right]\left(w_{3,\xi}^2 + 2w_{2,\xi}w_{4,\xi} - 2u_{3,\xi}w_{2,\xi}^2\right)_{,\xi} + \tfrac{1}{2}EA_{\epsilon 2}\left(w_{2,\xi}^2\right)_{,\xi} - EA_{z2}\left[w_{4,\xi\xi} - \tfrac{3}{2}\left(w_{2,\xi}{}^3\right)_{,\xi}\right] \tag{37}$$

$$w_{2,\xi\xi\xi\xi} - w_{2,\xi\xi} = 0 \tag{38}$$

$$w_{3,\xi\xi\xi\xi} - w_{3,\xi\xi} = 0 \tag{39}$$

$$w_{4,\xi\xi\xi\xi} - w_{4,\xi\xi} = P_2 - w_{2,00} + EA_{\epsilon 2}w_{2,\xi\xi} + \left[\left(c_1^2/c_2^2\right) - 1\right]\left(u_{3,\xi}w_{2,\xi} + \tfrac{1}{2}w_{2,\xi}^3\right)_{,\xi} - EA_{z2}u_{3,\xi\xi\xi} \tag{40}$$

Similarly, the inner expansions for the other end ($x = 1$) of the beam can be derived using the stretching transform $\zeta = (1 - x)/\varepsilon$:

$$-\left(c_1^2/c_2^2\right)u_{3,\zeta\zeta} = -\tfrac{1}{2}\left[\left(c_1^2/c_2^2\right) - 1\right]\left(w_{2,\zeta}^2\right)_{,\zeta} + EA_{z2}w_{2,\zeta\zeta\zeta} \tag{41}$$

$$-\left(c_1^2/c_2^2\right)u_{4,\zeta\zeta} = -\left[\left(c_1^2/c_2^2\right) - 1\right](w_{2,\zeta}w_{3,\zeta})_{,\zeta} + EA_{z2}w_{3,\zeta\zeta\zeta} \tag{42}$$

$$-\left(c_1^2/c_2^2\right)u_{5,\zeta\zeta} = -u_{3,00} + 2P_2 w_{2,\zeta} - \tfrac{1}{2}\left[\left(c_1^2/c_2^2\right) - 1\right]\left(w_{3,\zeta}^2 + 2w_{2,\zeta}w_{4,\zeta} + 2u_{3,\zeta}w_{2,\zeta}^2\right)_{,\zeta} - \tfrac{1}{2}EA_{\epsilon 2}\left(w_{2,\zeta}^2\right)_{,\zeta} + EA_{z2}\left[w_{4,\zeta\zeta} - \tfrac{3}{2}\left(w_{2,\zeta}^3\right)_{,\zeta}\right]_{,\zeta} \tag{43}$$

$$w_{2,\zeta\zeta\zeta\zeta} - w_{2,\zeta\zeta} = 0 \tag{44}$$

$$w_{3,\zeta\zeta\zeta\zeta} - w_{3,\zeta\zeta} = 0 \tag{45}$$

$$w_{4,\zeta\zeta\zeta\zeta} - w_{4,\zeta\zeta} = P_2 - w_{2,00} + EA_{\epsilon 2}w_{2,\zeta\zeta} - \left[\left(c_1^2/c_2^2\right) - 1\right]\left(u_{3,\zeta}w_{2,\zeta} - \tfrac{1}{2}w_{2,\zeta}^3\right)_{,\zeta} + EA_{z2}u_{3,\zeta\zeta\zeta} \tag{46}$$

This system, represented by string equations in the outer region and beam equations in the inner regions, is linear at all levels, self-adjoint, and solvable. Because the membrane is mounted using an elastic ring, torsional spring boundary conditions K_0 and K_L appear more accurate than a clamped condition. This model can also represent a region between the edge of the membrane and the beginning of the piezoelectrically actuated region. This also can be viewed as an additional control mechanism. When these dimensional boundary conditions are scaled and expanded,

$$u(0) = 0, \qquad u_{,x}(0) = 0, \qquad w(0) = 0$$
$$EIw_{,xx}(0) = N_z - EA_{\epsilon z} - K_0 w_{,x}(0) + EA_z\left(u_{,x} + \tfrac{1}{2}w_{,x}^2 - \tfrac{1}{8}w_{,x}^4 - \tfrac{1}{2}u_{,x}w_{,x}^2 + \tfrac{1}{2}u_{,x}^2 w_{,x}^2\right) \tag{47}$$

$$u(L) = 0, \qquad u_{,x}(L) = 0, \qquad w(L) = 0$$
$$EIw_{,xx}(L) = N_z - EA_{\epsilon z} + K_L w_{,x}(L) - EA_z\left(u_{,x} + \tfrac{1}{2}w_{,x}^2 - \tfrac{1}{8}w_{,x}^4 - \tfrac{1}{2}u_{,x}w_{,x}^2 + \tfrac{1}{2}u_{,x}^2 w_{,x}^2\right) \tag{48}$$

When the same scaling presented earlier is used, the following nondimensional boundary conditions are derived for the $x = 0$ end of the beam:

$$u_3(0) = 0, \qquad u_{3,\xi}(0) = 0, \qquad u_4(0) = 0$$

$$u_{4,\xi}(0) = 0, \qquad u_5(0) = 0, \qquad u_{5,\xi}(0) = 0 \tag{49}$$

$$w_2(0) = 0, \qquad N_0^2 w_{2,\xi\xi}(0) = -K_0 w_{2,\xi}(0)$$

$$w_3(0) = 0, \qquad N_0^2 w_{3,\xi\xi}(0) = -K_0 w_{3,\xi}(0) - EA_{\epsilon z 3}$$

$$w_4(0) = 0, \qquad N_0^2 w_{4,\xi\xi}(0) = -K_0 w_{4,\xi}(0) + EA_{z2} u_{3,\xi} \tag{50}$$

and at the $x = 1$ (scaled) end of the beam

$$u_3(0) = 0, \qquad u_{3,\zeta}(0) = 0, \qquad u_4(0) = 0$$

$$u_{4,\zeta}(0) = 0, \qquad u_5(0) = 0, \qquad u_{5,\zeta}(0) = 0 \tag{51}$$

$$w_2(0) = 0, \qquad N_0^2 w_{2,\zeta\zeta}(0) = -K_1 w_{2,\zeta}(0)$$

$$w_3(0) = 0, \qquad N_0^2 w_{3,\zeta\zeta}(0) = -K_1 w_{3,\zeta}(0) - EA_{\epsilon z 3}$$

$$w_4(0) = 0, \qquad N_0^2 w_{4,\zeta\zeta}(0) = -K_1 w_{4,\zeta}(0) + EA_{z2} u_{3,\zeta} \tag{52}$$

where it can now be seen that $EA_{\epsilon z 3}$ represents the nondimensional moment imposed by the piezoelectric layer(s) and $N_z = 0$ using the neutral axis. This research is concerned with both the dynamic properties of this material and its static shape manipulation capabilities. At this point, to study the shaping capabilities of the system, only the static solution is necessary.

Static Shaping

When it is noted that the system is now separated, the axial solution, u, is completely determined by the lower-order transverse solution, w. We can solve the system of equations, using a two-level matching, to find the following composite solution to order ε^3:

$$u^c(x) = 0$$

$$w^c(x) = \varepsilon^2 (P_2/2)(x - x^2) - \varepsilon^3 (\Gamma_0 \{1 - x - \exp[-(x/\varepsilon)]\}$$

$$+ \Gamma_1 \{x - \exp[-(1 - x)/\varepsilon]\}) \tag{53}$$

where

$$\Gamma_0 = \frac{K_0}{K_0 - N_0^2}\left[\frac{P_2}{2} + \frac{EA_{\epsilon z 3}}{K_0}\right]$$

$$\Gamma_1 = \frac{K_1}{K_1 - N_0^2}\left[\frac{P_2}{2} + \frac{EA_{\epsilon z 3}}{K_1}\right] \tag{54}$$

From this solution, we can see the axial distortion is not present to order ε^3. We will neglect the axial displacement to this level because the smallness factor is roughly the ratio of thickness to length in the system of interest. Note that the axial displacement equation is not trivial at the next order.

Figures 5 and 6 show the behavior of the piezoelectric laminate beam with no pressure differential and symmetric edge conditions. Using a 15-cm-long, simple three-layer laminate with the base layer of Kapton® and two layers of PVDF with the properties listed in Table 1, we applied reasonable environmental and actuation values to yield interesting results.

Actuation causes a pistoning of the center portion of the beam a total of approximately a wavelength of visible light that corresponds

Table 1 Material properties

Property	Kapton	PVDF
Modulus E, GPa	2.8 GPa	1.8 GPa
Thickness H, μm	100 micron	50 micron
Piezocoefficient d_{31}, pC/N	——	−16

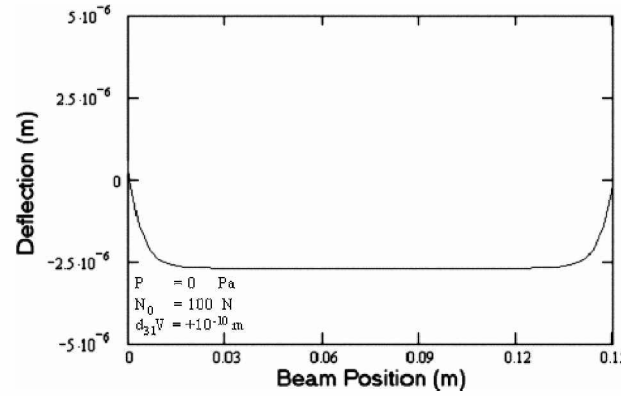

Fig. 5 Piezoelectric (+) beam deflection.

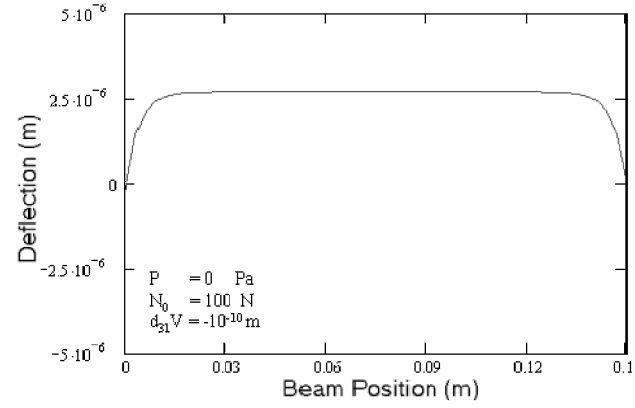

Fig. 6 Piezoelectric (−) beam deflection.

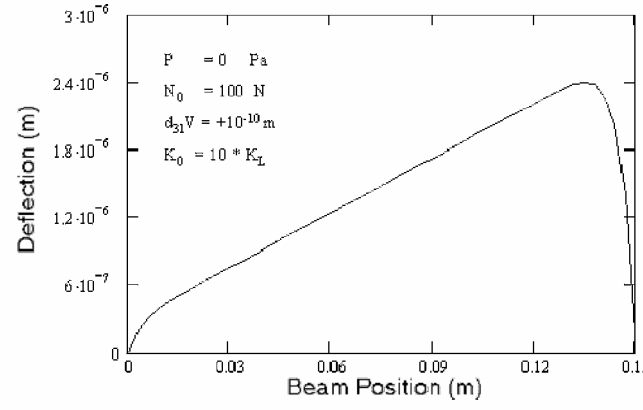

Fig. 7 Edge control.

favorably with experimental observations.[3] The effective boundary-layer region is approximately of the order of $\sqrt{\varepsilon}$, as expected from the original mathematical foundation. Because ε is inversely proportional to square root N_0, it is clear the boundary region will grow as the pretension is decreased. However, this statement is limited to the underlying assumptions of the asymptotic method. If the pretension is reduced to the point where $\varepsilon \ll L$ is violated, the method breaks down, and the results can no longer be assumed valid.

Because the center outer region of the beam behaves as a string, incapable of countering any bending moment, this region can only produce a linear contribution. With the inner regions providing the necessary bending stiffness to counter the piezomoment applied, these boundary regions produce significant curvature changes.

The result of dissimilar edge stiffness is shown in Fig. 7. With the use of a combination of edge control of the stiffness represented by the K_0 and K_1 terms and piezoelectric laminate actuation, a reflected wave front can be modified by over a wavelength of tilt. Again notice the boundary region effects are the same magnitude as the symmetric case discussed earlier.

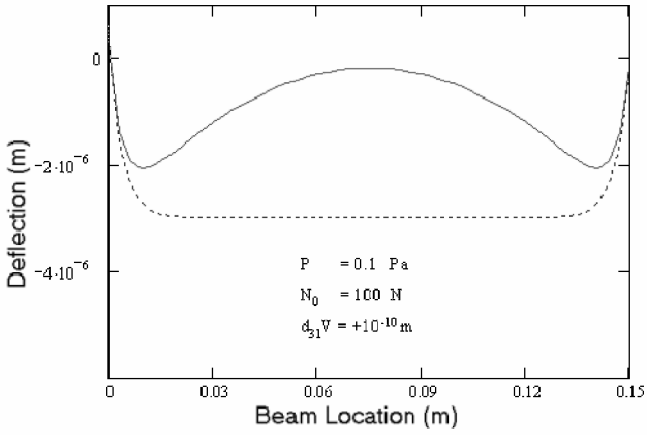

Fig. 8 Piezoelectric (+) beam deflection.

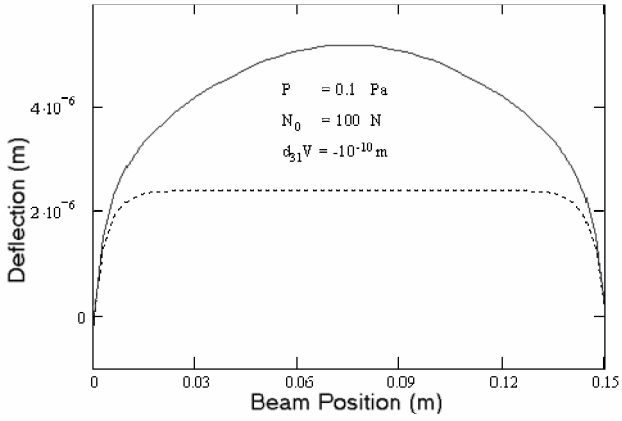

Fig. 9 Piezoelectric (−) beam deflection.

If the beam is has a small pressure differential applied, similar results are possible. Symmetric edge conditions and actuation result in additional curvature alteration (Figs. 8 and 9). The dashed line represents the actual surface deflection given the applied conditions, whereas the solid line indicates the effective surface change due to the applied piezo effect. In this case, the wave front modification appears to be of a defocus type, when it is considered that the usable reflective surface would be the center 70–80% of the circular region. Note that different edge conditions results in additional tilt behavior as seen in the nonpressurized system and can be applied as a simple superposition of effects. The difference between the symmetric and unsymmetric cases appear linear across the surface. With the static shaping capabilities understood, we can now study the dynamic nature of the laminate.

Dynamic Response

As discussed in the preceding section, the axial equations, u, are decoupled from the transverse equations, w, when the system is scaled and expanded as in this paper. Solving the system of equations at order ε^2 and eliminating any terms linear in time yields a simple string:

$$w_2^c(x) = \frac{P_2}{2}(x - x^2) + \sum_{i=1}^{\infty} a_{1n}(T_1)\{\exp[i\beta_{n0}(T_0 + x)] - \exp[i\beta_{n0}(T_0 - x)] + cc\} \tag{55}$$

where $\beta_{n0} = n\pi$ and $a_{1n}(T_1)$ can be a function of $T_1, T_2, \ldots$ and is yet to be determined. We now concentrate on the solution for next level of equations at order ε^3. Because this system is self-adjoint, we apply the Fredholm alternative theorem (see Ref. 9) to derive the necessary solvability conditions. As a result, the $a_{1n}(T_1)$ coefficients in Eq. (55), as well as ω_1, can be determined based on the applied boundary conditions.

We will concern ourselves with two different conditions: constant and periodic forcing. The forcing is applied through the thermal and electrical parameters:

$$EA_{\epsilon 2} = f_0 + f\sin[(\Omega + \varepsilon\delta)t] = f_0 + f\sin(\Omega T_0 + \delta T_1)$$
$$EA_{\epsilon z 3} = m_0 + m\sin[(\Omega + \varepsilon\delta)t] = m_0 + m\sin(\Omega T_0 + \delta T_1) \tag{56}$$

Here we will concern ourselves with two values of Ω: β_{j0} and $2\beta_{j0}$, or odd and even modes. To the order studied in this paper, these selections represent a complete set of possible solutions.

Applying the solvability conditions, which require cancellation of all modes existing in Eq. (55), results in the following:

$$\omega_1 = -(1/\beta_{n0})(\delta - i\mu_1) \tag{57}$$

$$a_{1k} = 0 \qquad (k \neq j)$$
$$= A_{1k}e^{i\delta T_1} \qquad (k = j) \tag{58}$$

where

$$A_{1k} = \frac{m}{2\beta_{k0}}\left[\frac{\left(K_1 - N_0^2\right) - (-1)^k\left(K_0 - N_0^2\right)}{K_1\left(K_0 - N_0^2\right) + K_0\left(K_1 - N_0^2\right)}\right] \tag{59}$$

It is now clear, with symmetric boundary conditions, that only the odd mode exists at this level. The solution for the next level transverse displacement is then

$$w_3^c(x) = -\frac{P_2}{2}\left[\frac{K_0}{K_0 - N_0^2}\right][1 - x - \exp(-\xi)] - \frac{P_2}{2}\left[\frac{K_1}{K_1 - N_0^2}\right][x + \exp(-\zeta)] - a_{1k}\beta_{j0}\left[\frac{K_0}{K_0 - N_0^2}\exp(-\xi) - (-1)^k\frac{K_1}{K_1 - N_0^2}\exp(-\zeta)\right]\sin(\beta_{j0}T_0) - m\left[\frac{1}{K_0 - N_0^2}\exp(-\xi) - (-1)^k\frac{1}{K_1 - N_0^2}\exp(-\zeta)\right]\sin(\beta_{j0}T_0 + \delta T_1) + \sum_{i=1}^{\infty}\{a_{2n}(T_1)\exp[i\beta_{n0}(T_0 + x)] + a_{3n}(T_1)\exp[i\beta_{n0}(T_0 - x)] + cc\} \tag{60}$$

As in the static solution, the axial displacement solution is trivial to this level, and so we will neglect it in this analysis.

Applying the preceding results to the next level, we can again derive the necessary solvability conditions, which require cancellation of all modes existing in both the previous levels. The results of interest are

$$\omega_2 = \left(1/\beta_{n0}^2\right)\left(\mu_1^2 + 2\delta^2 + \beta_{n0}^4 - f_0\beta_{n0}^2\right) \qquad (\Omega = \beta_{j0})$$
$$= \left(1/\beta_{n0}^2\right)\left[\mu_1^2 + 2\delta^2 + \beta_{n0}^4 - f_0\beta_{n0}^2 - (f/2)\beta_{n0}^2\exp(i\delta T_1)\right] \qquad (\Omega = 2\beta_{j0}) \tag{61}$$

$$a_{2k} = 0 \qquad (k \neq j), \qquad a_{2k} = A_{2k}\exp(i\delta T_1) \qquad (k = j)$$
$$a_{3k} = -\bar{a}_{2k} \tag{62}$$

where

$$A_{2k} = \frac{fP_2}{2\beta_{k0}^2} + i\frac{m}{K_0 - N_0^2} \times \left\{1 - K_0\left[\frac{\left(K_1 - N_0^2\right) - (-1)^k\left(K_0 - N_0^2\right)}{K_1\left(K_0 - N_0^2\right) + K_0\left(K_1 - N_0^2\right)}\right]\right\} \tag{63}$$

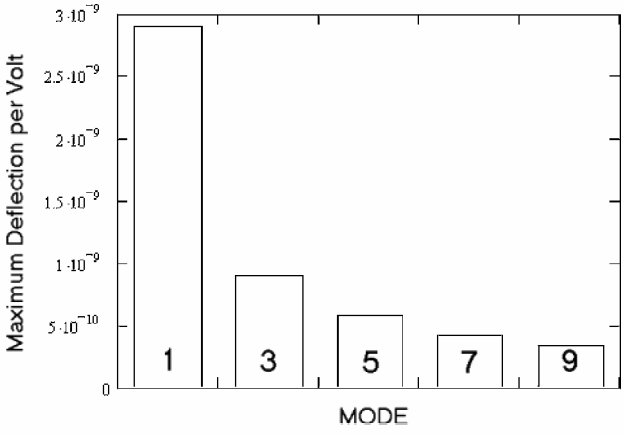

Fig. 10 Maximum dynamic deflection.

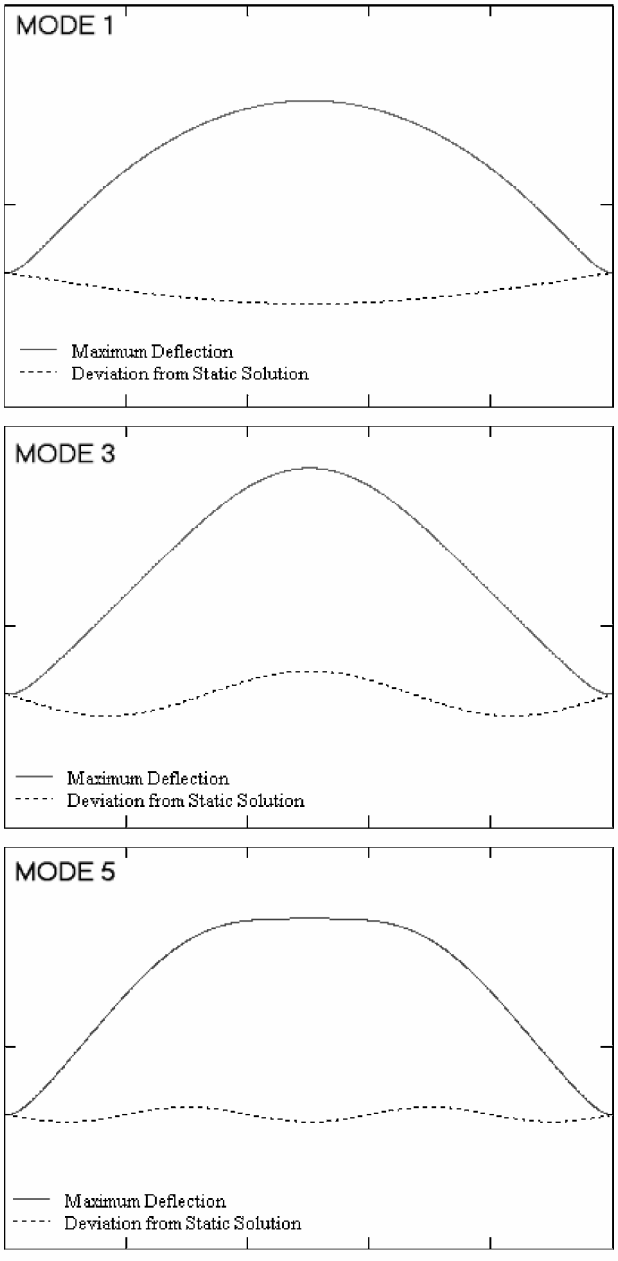

Fig. 11 Odd mode shape results: pressurized beam string.

Applying these results, and the original scaling used, we can derive the dimensional results. With the assumption of an odd driving frequency ($n =$ odd), the modal frequency for the beam string is now

$$\beta_n = (n\pi + \delta)\omega^*\left(\sqrt{N/\rho AL^2}\right) \tag{64}$$

where

$$\omega^* = 1 - \varepsilon(\delta/n\pi) + \varepsilon^2[1/2(n\pi)^2]\left[\mu_1^2 + 2\delta^2 + (n\pi)^4 - f_0(n\pi)^2\right] \tag{65}$$

which illustrates the difference (to this level) of the piezothermoelectric beam-string frequencies from the standard string frequencies: $\beta_n = n\pi\sqrt{(N/\rho AL^2)}$.

Maximum deflection per volt applied to the laminate described here is presented in Fig. 10. Because we select the higher modes, the resultant deflection gets progressively smaller, as expected. The first three odd mode shapes (even modes are trivial) of a pressurized beam string are presented is Fig. 11. The solid line indicates the actual shape of the beam, whereas the dotted line presents the dynamic variation, which is superimposed on the static displacement.

Conclusions

The static and dynamic solutions to a nonlinear, pressurized, piezothermoelastic beam string were developed. The results indicate the piezoelectric effect can be modeled effectively as an in-plane stretching term coupled with a boundary moment term. The moment term causes localized curvature effects that are compensated for with the in-plane terms. The results were used to analyze a Kapton/PVDF beam, which illustrate the effectiveness of such a mechanism at optical wavelengths.

The analysis of compliant structures, such as inflatable space structures, requires a departure from the standard methods. The difficulties inherent with the very large-scale differences cause instabilities when classical methods are applied. This is the first of a series of papers leading to a new methodology that may provide analysts with a tool capable of efficiently analyzing such troublesome structures.

Acknowledgments

This work was supported by the Air Force Office of Scientific Research, Brian Sanders and Daniel Segalman monitoring. Additionally, we would like to thank William Baker for his insights and suggestions throughout the development of the results presented.

References

[1]Cassapakis, C., and Thomas, M., "Inflatable Structures Technology Development Overview," AIAA Paper 95-3738, Sept. 1995.

[2]Freeland, R., and Veal, G., "Significance of the Inflatable Antenna Experiment Technology," AIAA Paper 98-2104, April 1998.

[3]Wagner, J., "Optical Metrology of Adaptive Membrane Mirrors," M.S. Thesis, U.S. Air Force Inst. of Technology, Wright–Patterson AFB, OH, March 2000.

[4]Main, J., Nelson, G., and Martin, J., "Electron Gun Control of Smart Structures," *Smart Structures and Integrated Systems*, Vol. 3329, Society of Photo-Optical Instrumentation Engineers (International Society for Optical Engineering), Bellingham, WA, 1998, pp. 688–693.

[5]Agnes, G., and Wagner, J., "Adaptive Structures Technology for Membrane Optical Surfaces," AIAA Paper 2001-1199, April 2001.

[6]Cook, R., Malkus, D., and Plesha, M., *Concepts and Applications of Finite Element Analysis*, 3rd ed., Wiley, New York, 1974, pp. 75–78.

[7]Nayfeh, A., and Mook, D., *Nonlinear Oscillations*, Wiley, New York, 1979, pp. 447–455.

[8]Nayfeh, A., *Introduction to Perturbation Techniques*, Wiley, New York, 1981.

[9]Stakgold, I., *Green's Function and Boundary Value Problems*, 2nd ed., Wiley, New York, 1998, pp. 228–232.

C. Jenkins
Guest Editor